Energetics of heterometal substitution in ε-Keggin $[MO_4Al_{12}(OH)_{24}(OH_2)_{12}]^{6/7/8+}$ ions

(Revision 2)

Dana Reusser[1], William H. Casey[2], and Alexandra Navrotsky[1*]

[1]Peter A. Rock Thermochemistry Laboratory and NEAT ORU, University of California at Davis, Davis, California 95616, U.S.A. *E-mail: anavrotsky@ucdavis.edu

[2]Department of Chemistry, Department of Geology, University of California at Davis, Davis, California 95616, U.S.A.

Abstract: Aluminum hydroxide ions in the ε-Keggin structure provide geochemical models for how structure affects reactivity, and consequently, how aqueous ions evolve to bulk precipitates. Here we report a systematic comparison of heterometal substitution into the MAl_{12} ε-Keggin structure, where M = Ga^{III}, Al^{III}, or Ge^{IV}. We use direct solution calorimetric techniques to compare the energetics of these substituted structures and complement these measurements with density functional theory, DFT, calculations to further examine this structure as a host to alternative heterometals. The measured enthalpy of solution, ΔH_{soln}, at 28 °C in 5 N HCl for the selenate salts of $GaAl_{12}^{7+}$ and $AlAl_{12}^{7+}$, was measured as -869.71 ± 5.18 and -958.04 ± 2.79 kJ·mol^{-1}, respectively. The enthalpies of formation from the elements, $\Delta H^{\circ}_{f,el}$, for the selenate salts of $GaAl_{12}^{7+}$ and $AlAl_{12}^{7+}$, are -23334.18 ± 60.38 and -23075.02 ± 61.68 kJ·mol^{-1}, respectively, supplanting previous values. We compare structural relationships to both experimental and calculated energies to identify the driving forces that control these substitutions and stability, and establish that tetrahedral M-O bond lengths are closely related to the strain and stability of the structure. We show that substitution depends on the size and valence of the

heterometal through energetics, and we extend our thermodynamic and structural relationships to other not yet synthesized MAl_{12} clusters (M = Si^{IV}, Fe^{III}, Be^{II}, Mg^{II}, or Zn^{II}).

Keywords:thermodynamics, calorimetry, DFT, ε-Keggin, aluminium hydroxide, Al_{13}

Introduction

Geochemists are intensely interested in understanding the ligand and electron exchange reactions affecting minerals in soil and water. These minerals are often oxide and hydroxide phases of iron and aluminum and have dimensions of a few nanometers to micrometers. These materials are in chemical communication with the adjacent aqueous solutions and provide a key pathway for detoxifying natural waters (Furrer et al., 2002; Stewart et al., 2009). Similar oxides are important in materials science, with applications largely in catalysis.

One approach to understanding mineral oxide reactions is to employ large metal hydroxide ions as experimental models and then probe near-elementary reactions via molecular spectroscopies to discover general rules describing reactivity (Casey and Rustad, 2007). A good example is provided by the aluminum hydroxide ions in the ε-Keggin structure (Fig. 1). These ions expose to solution some of the same aluminum - oxygen coordination chemistries that are found in soil minerals. Such ions are much better constrained for experiments than a colloidal suspension of solids where the surface structures are incompletely known. Correspondingly, experiments on the ions have identified general controls of isotope-exchange kinetics that undoubtedly affect larger oxide structures as well. For example, oxygen-isotope exchange into bridging oxygens in these large aluminum hydroxide ions proceeds via metastable structures that form by partial detachment of metal atoms from deeper structural oxygens (Rustad et al., 2004). This partly detached intermediate accepts addition of an isotopically distinct solvent oxygen to

the undercoordinated metal before condensing back into the stable form (Rustad and Casey, 2012). The extent to which these intermediates form is extraordinarily sensitive to heteroatom substitutions in the inert core of the stable molecule, well away from the sites of oxygen-isotope exchange. By suppressing or enhancing the metastable equilibrium, these single-atom substitutions exert a disproportionate influence over the kinetics of isotope-exchange reactions throughout the structure (Rustad et al., 2004). This idea has been extended to other classes of oxide clusters (Rustad and Casey, 2012) and the authors argue from them that it is ensembles of metastable intermediates, and not hypothetical transition states, that control rates of both isotope-exchanges and dissociations at the solution-oxide interface.

Here we suggest the feasibility of making other heteroatom substitutions in the MAl_{12} class of polyoxocations (Johansson, 1960), having the stoichiometry $[MO_4Al_{12}(OH)_{24}(H_2O)_{12}]^{6/7/8/+}$ and having the ε-isomer structure of the Baker-Figgis-Keggin series (Baker and Figgis, 1970; Keggin, 1933). The only structures that have been isolated so far have $M=Al^{III}$, Ga^{III}, or Ge^{IV}. We build upon our previous thermochemical examination of the stability of these clusters (Armstrong et al., 2011) and provide new thermochemical data to complement theoretical energetic calculations to suggest new potential compositions. We also correct our previously reported values for the $AlAl_{12}$ selenate salt, as we realized in this Armstrong et al. 2011 paper, the stoichiometries omitted ~12 moles of water per structure. In the subsequent text, we use the nomenclature that $GaAl_{12}$, $AlAl_{12}$ and $GeAl_{12}$ correspond to versions of the molecule, but always in the ε-isomer structure of the Baker-Figgis-Keggin series.

Experimental Methods

Synthesis and characterization

We characterized the selenate salts of $[MO_4)Al_{12}(OH)_{24}(H_2O)_{12}]^{7/8+}$, where $M=Al^{III}$, Ga^{III}, or Ge^{IV}, using powder X-ray diffraction (PXRD), thermogravimetric analysis (TGA), and solid-state ^{27}Al magic angle spinning nuclear magnetic resonance (MAS NMR) spectroscopy. Additionally, we collected single crystal X-ray diffraction (SXRD) data on the $AlAl_{12}$ and $GaAl_{12}$ selenate salts. More details on the synthesis and characterization can be found in the supporting information.

Solution calorimetry

A Setaram C-80 calorimeter was used to measure the enthalpies of solution, ΔH_{soln}, of the $MAl_{12}^{7/8+}$ salts and reference materials according to methods established previously (Armstrong et al., 2011). Solid samples were dropped from room temperature directly into hydrochloric acid (5.00 g, 5 N) held at 28 °C. The calorimeter was calibrated using the measured enthalpy of solution of KCl (NIST SRM 1655) in deionized water. The sample mass of each run was carefully controlled to ensure that the same final molality was achieved. We also needed to obtain the enthalpy of formation for one of the reference materials using high temperature oxide melt solution calorimetry, and these details are in the supporting information.

Computational methods

The geometries and thermochemistry of the heterometal-substituted $MAl_{12}^{6/7/8+}$ and their associated tetrahedral metal hydroxides were calculated using density functional theory (DFT). These calculations were performed using Gaussian 09 (Frisch et al., 2009) at the level of 6-31g* to optimize the geometries of the clusters and model the thermodynamic exchange reaction on the aqueous and gaseous MAl_{12} clusters. The restricted b3lyp (Becke, 1993; Stephens et al., 1994), a hybrid generalized gradient approximation (GGA) exchange-correlation functional, was

used for all species with the exception of the paramagnetic iron cluster, where an unrestricted b3lyp (Becke, 1993; Stephens et al., 1994) exchange-correlation functional was used and limited to high-spin Fe^{III}. We chose to use the b3lyp method for all of the thermochemical calculations in this work, as it provided more accurate enthalpies of exchange and is well established in predicting thermochemistries (Sousa et al., 2007; Wong, 1996; Zhao and Truhlar, 2008). The MAl_{12} geometries were also optimized using SVWN5 (Vosko et al., 1980), a local density approximation (LDA) at the 6-31g* level. We use this method to calculate the tetrahedral core bond lengths in the subsequent text and calculations, as it provides an accurate prediction of these bond lengths in the MAl_{12} clusters to ± 0.01 Å. All MAl_{12} clusters except $FeAl_{12}$ converged to T_d symmetry, but no symmetry was forced in the calculations. A polarizable continuum model (PCM) was used for the aqueous solvent for all optimizations and frequency calculations (Frisch et al., 2009).

Results and Discussion

Synthesis and characterization

Powder X-ray diffractograms (PXRD) of the $MAl_{12}^{7/8+}$ crystalline products (Fig. S1) show sharp diffraction peaks in the 5-65° 2θ region. The $GeAl_{12}$ selenate was matched to the crystal information file (cif) obtained from the results of (Lee et al., 2001) with no visible extraneous peaks (Fig. S1c). Similarly, the $AlAl_{12}$ and $GaAl_{12}$ selenates were matched to the powder diffraction file (PDF) #76-1750 (Johansson, 1960) with no additional peaks present (Fig. S1a,b). Additionally, single crystal diffraction (SXRD) shows that the $AlAl_{12}$ and $GaAl_{12}$ selenate products are also free of impurities and are isostructural. We use our values for the tetrahedral <M-O> bond lengths in the $AlAl_{12}$ and $GaAl_{12}$ selenates throughout the text as they

correspond well with those measured by Parker et al., 1997 (Table 1). The PXRD diffractograms (Fig. S1) and results of the TGA and MAS NMR can be found in the supporting information.

Solution calorimetry

To examine how heterometal substitution influences the structure and the relative stability of the $AlAl_{12}$, $GaAl_{12}$, and $GeAl_{12}$ clusters, we compare the exchange reactions (*Reactions 1-3*) between substituted clusters using measured enthalpies of solution, ΔH_{soln}. The difference between these ΔH_{soln} gives the enthalpies of exchange, ΔH_{ex}, of the heterometals in the tetrahedral site in the molecule. This provides a measure for the strain observed in the isostructural or nearly isostructural MAl_{12} clusters (Fig. 1). The isothermal solution calorimetry data used for these calculations and those in the subsequent text are summarized in Table 1. The measured data from the solution calorimetry for all three $MAl_{12}^{7/8+}$ selenate compounds and reference materials are reported in Tables S2 and S4 with errors calculated as two standard deviations of the mean.

While the $AlAl_{12}$ and $GaAl_{12}$ solids are isostructural, the $GeAl_{12}$ solid is not. With a higher ionic charge, it lacks the sodium counterion observed in the tetrahedral aluminum- and gallium–centered MAl_{12} clusters. Therefore, the enthalpy of solution with sodium in the cycle was calculated for $GeAl_{12}$ in order to more accurately compare its thermochemistry to the $AlAl_{12}$ and $GaAl_{12}$ solids (Tables S3 and S4). This is the value we report in Table 1 and use for calculations throughout the text.

The reactions below give the enthalpy of exchange, ΔH_{ex}, between the experimental MAl_{12} and the heteroatoms:

131 *(1)* $Na[(AlO_4)Al_{12}(OH)_{24}(H_2O)_{12}](SeO_4)_4 \cdot 12H_2O_{(cr)} + Ga^{3+}_{(aq)} =$

132 $Na[(GaO_4)Al_{12}(OH)_{24}(H_2O)_{12}](SeO_4)_4 \cdot 12H_2O_{(cr)} + Al^{3+}_{(aq)}$

133 $\Delta H_{ex} = -88.33 \pm 5.88$ kJ·mol^{-1}

134 *(2)* $[(GeO_4)Al_{12}(OH)_{24}(H_2O)_{12}](SeO_4)_4 \cdot 12H_2O_{(cr)} + Al^{3+}_{(aq)} + NaOH_{(cr)} + 3H_2O_{(l)} =$

135 $Na[(AlO_4)Al_{12}(OH)_{24}(H_2O)_{12}](SeO_4)_4 \cdot 12H_2O_{(cr)} + 3H^{+}_{(aq)} + Ge(OH)_4{}^{0}_{(aq)}$

136 $\Delta H_{ex} = -17.15 \pm 11.85$ kJ·mol^{-1}

137 *(3)* $[(GeO_4)Al_{12}(OH)_{24}(H_2O)_{12}](SeO_4)_4 \cdot 12H_2O_{(cr)} + Ga^{3+}_{(aq)} + NaOH_{(cr)} + 3H_2O_{(l)} =$

138 $Na[(GaO_4)Al_{12}(OH)_{24}(H_2O)_{12}](SeO_4)_4 \cdot 12H_2O_{(cr)} + 3H^{+}_{(aq)} + Ge(OH)_4{}^{0}_{(aq)}$

139 $\Delta H_{ex} = -105.48 \pm 12.63$ kJ·mol^{-1}

140 **Computational results**

141 Because only three of these clusters have been characterized experimentally, we coupled
142 experimental measurements to computational work to expand our subset of heterometals. This
143 allowed us to look at the exchange reactions between the aqueous clusters and see how various
144 heterometals affect the geometry and thermochemistry of the clusters. We used two well
145 established exchange-correlation functionals to calculate the geometries of MAl_{12} clusters in this
146 work, both with a 6-31g* basis set and with a polarizable continuum model (PCM) for the
147 aqueous solvent (Frisch et al., 2009). These clusters have 101 atoms, thus a 6-31g* basis set was
148 chosen to optimize both accuracy and computing time. A local density approximation (LDA),
149 SVWN5 (Vosko et al., 1980), produced very accurate tetrahedral bond lengths compared to
150 experiment with a mean absolute error (MAE) of 0.01 Å (see Table 2). However, it did not
151 reproduce the exterior geometry of the MAl_{12} cluster as accurately or its thermochemistry

compared to experiment. Alternatively, the hybrid generalized gradient approximation (GGA) exchange-correlation functional, b3lyp (Becke, 1993; Stephens et al., 1994), showed contrasting results. This functional produced longer tetrahedral bond lengths (Table 2) compared to experiment with a MAE of 0.03 Å, but more accurate μ_4-O-Al^{III} bond lengths and thermochemistry. The converged geometries using both functionals are given according to their optimized tetrahedral M-O bond lengths in Table 2. We provide the Cartesian coordinates for all optimized structures in the supporting information.

For simplification, $GeAl_{12}$ was selected as a reference for comparison and all b3lyp thermochemical results are presented relative to the energies of this cluster (see Table 2). We used the sum of the electronic and thermal enthalpies for each MAl_{12} cluster and tetrahedral hydroxide to calculate the enthalpy of exchange reaction, ΔH_{ex}, with the $GeAl_{12}$ cluster according to the following reaction:

(4) $$GeAl_{12}^{8+} + M(OH)_4^{x-4} = MAl_{12}^{x+4} + Ge(OH)_4^{0}$$

where M = Si^{IV}, Ge^{IV}, Al^{III}, Ga^{III}, Fe^{III}, Be^{II}, Mg^{II}, or Zn^{II}; and x = the valence of the substituting heterometal, M.

We also provide the gas-phase exchange reactions in Table 2 to show that any trends are consistent and not an artifact of the PCM calculations. These gas phase reactions show the same general trend in the relative stabilities of the MAl_{12} clusters, which suggests that the incorporation of the solvent model does not affect the relative stabilities of the clusters. All other calculations and the subsequent discussion use the PCM model results for solvent shielding.

The b3lyp method did produce more exothermic aqueous enthalpies of exchange for the aqueous clusters, but the trend is quite similar compared to the experimental measurements

obtained on the solid clusters. These results are consistent with several reports on the accuracy of these methods for calculating thermochemistry and geometric features of chemical structures, where the b3lyp functional provides more accurate thermochemical predictions (Sousa et al., 2007; Wong, 1996; Zhao and Truhlar, 2008). In the subsequent discussion of the structure and stability of the MAl_{12} clusters, when we examine the tetrahedral core explicitly, we use the tetrahedral bond lengths obtained from the SVWN5 method because it was more accurate for this region. For the thermochemistry and cavity size including the adjacent μ_4-O-Al^{III} bond lengths, we use the results from the b3lyp method because this method is better known for its thermochemical predictions and agreed with our general experimental trends.

Heterometal influence on the tetrahedral core

DFT and calorimetric measurements on this isomer of the Keggin structure show that the stability and structure depends on the valence and the size of the substituting heterometal. Specifically, when the (1) *valence* of the substituting heterometal creates a lower-charged aqueous MAl_{12} cluster, this species is more stable relative to the higher charged species. (2) Within isovalent series of MAl_{12} clusters in the ε-Keggin structure, the *size* of the substituting heterometal influences the cluster's stability. Going down the periodic table to the 4^{th} period, the MAl_{12} ions in the ε-Keggin structure become increasingly stable within each isovalent group, i.e, for the divalent cations, the substituted clusters exhibit increasingly more exothermic ΔH_{ex} with $GeAl_{12}^{8+}$ going from heteroatoms Be^{2+} to Mg^{2+}, to Zn^{2+}(see Table 2).

The M-μ_4-O bond length, and the adjacent distance between the μ_4-O-Al^{III} composing the trimeric groups of the clusters (Fig. 2a), depend on the nature of the heterometal in these MAl_{12} structures. We show how these bond lengths are affected by using a radius of the cluster,

196 alternatively the tetrahedral cavity, that incorporates both of these bonds. This distance is
197 denoted as, *d*, in Figure 2a. To examine the role of heterometal on the size and the relative
198 stability of these clusters, we compare enthalpy of exchange between substituted clusters to the
199 radius, *d*. The influence of heterometal size to the structure stability is particularly evident in the
200 experimental exchange reaction between the isostructural $AlAl_{12}$ and $GaAl_{12}$ clusters seen in
201 *Reaction (1).* In this reaction, by substituting Ga^{III} for Al^{III} in the MAl_{12} structure, the
202 isostructural heptavalent $GaAl_{12}$ cluster is $-88.33 \pm 5.88\ kJ{\cdot}mol^{-1}$ more stable in enthalpy than the
203 $AlAl_{12}$ cluster. The distance, *d*, from the heterometal to the trimeric group plane in the cluster
204 expands from 2.95 Å in $AlAl_{12}$ to 2.97 Å in $GaAl_{12}$. The ε-Keggin structure contains four
205 trimeric groups, so this expansion would actually occur by 0.02 Å in four locations throughout
206 the structure. This expansion in the structure, coupled with a significant exothermic exchange
207 reaction enthalpy, provides convincing evidence that the size of the heterometal is a major factor
208 in the stability of the ε-Keggin structure.

209 By extending this practice to all three of the measured clusters, and then comparing the
210 ΔH_{ex} with $GeAl_{12}$ to our metric for the cluster radius, we created an experimental guideline for
211 our computational work to look at how substitution with other heterometals affects the geometry
212 and relative stability of new potential structures. In Figure 2b, we show the results of these
213 comparisons. We see in Figure 2b, that our results from the b3lyp calculations follow a similar
214 pattern as our experimental work. Of the three experimentally determined clusters, both methods
215 show that the $AlAl_{12}$ cluster has the smallest distance to its trimeric group plane and that
216 substitution with gallium results in stabilization with a lengthening in *d*. Substituting germanium
217 increases this distance, *d*, to the upper limit observed in both methods and decreases the stability
218 in terms of enthalpy. This order of stability also corresponds to reactivity of hydroxo bridges to

isotope exchange, as noted before (Rustad et al., 2004). While all of the b3lyp results are shifted to higher *d* values because of the longer calculated M-O bond lengths, this method overestimates this distance, *d*, for all of the known experimental clusters, and it also overestimates all of the M-O bond lengths for the theoretical clusters compared to the SVWN5 method, which is accurate to ± 0.01 Å for this bond length. Our boundary for the upper and lower limits of the cluster radius size is based strictly on the calculated clusters, knowing that *all* of their *d* values are overestimated. This range is exhibited by the vertical dashed lines in Figure 2b. Now, when looking for the theoretical clusters which fall within this range, we see that Be produces a cavity that is too small and lies to the far left of the vertical dashed lines, while Si produces a cavity that is too large for this structure. All of the other heteroatoms lie within, or close to the exhibited range.

Tetrahedral strain

A major contributing component to the distance, *d*, is the tetrahedral M-μ_4-O bond length, which accounts for over 60% of the distance to the trimeric group plane. To maintain tetrahedral symmetry, the exterior framework of twelve Al^{III} cations must expand and contract around the tetrahedral core. Consequently, there are drastic elongations of the M-μ_4-O bond length. In the simplest sense, the structure will favor heterometals that prefer longer tetrahedral bond lengths. To determine the tetrahedral bond lengths for each of the heterometals used in this study, we established normal distributions of tetrahedral M-O bond lengths found in dozens to hundreds of tetrahedrally coordinated structures in the Cambridge Crystal Structure Database (CCSD) (Allen, 2002) (Fig. 3). To check the accuracy of these distributions, we compiled the tetrahedral M-O bond lengths for common minerals with each of the substituted heterometals in this study (Table 3). All of the bond lengths from the mineral structures in Table 3 easily lie

242 within these distributions on Figure 3, but many of the predicted M-μ_4-O bond lengths in the ε-
243 isomer of the Keggin structure lie far from their corresponding mean bond lengths. We
244 emphasize that here we refer to SVWN5 results and use this method in Figure 3 because of the
245 better agreement with the measured bond lengths, as previously noted.

246 We observe that there are lower deviations between the MAl_{12} M-O bond lengths and the
247 mean of its corresponding distribution going towards longer tetrahedral bond lengths in Figure 3.
248 It is evident that our former assumption of the MAl_{12} structure favoring heterometals with longer
249 average tetrahedral M-O bond lengths is confirmed by the data presented in Figure 3. The
250 experimental Ga^{III} –centered structure is the most stable of the known structures, and also possess
251 the longest average M-O bond length of the three experimental clusters, $GaAl_{12}$, $AlAl_{12}$, and
252 $GeAl_{12}$. The distribution for tetrahedral Mg-O bond lengths is not shown on Figure 3, because
253 only a handful of tetrahedrally coordinated compounds could be found under our constraints in
254 the CCSD, but the Mg-centered cluster geometry can be compared to the tetrahedral M-O bond
255 lengths in the spinel structure given in Table 3. This difference between the $MgAl_{12}$ tetrahedral
256 M-O bond lengths and the $MgAl_2O_4$ M-O bond lengths, 0.072 Å, is similar in magnitude to the
257 deviation observed in the $GaAl_{12}$ cluster. Second, Figure 3 also suggests that regardless of
258 choice of heterometal, the ε-isomer of the Keggin structure is strained at its tetrahedral site
259 compared to other oxide minerals with tetrahedral coordination. The least strained clusters
260 appear to be the theoretical $ZnAl_{12}$ and $FeAl_{12}$ clusters. These two heterometals in the ε-isomer
261 of the Keggin structure have M-O bond lengths that lie closest to the means of their distributions.
262 The strained MAl_{12} tetrahedral bond lengths further support that most of these clusters are indeed
263 metastable species with respect to oxyhydroxide phases (Armstrong et al., 2011) .

264 **Implications**

Potential structures

$ZnAl_{12}$ and $FeAl_{12}$ are the most feasible heterometal-substituted clusters in terms of bond lengths and calculated energies. Figure 2b shows that the $ZnAl_{12}$ cluster's radius is slightly larger than that of the b3lyp tetrahedral $GeAl_{12}$ cluster, but as a hexavalent cluster, it is predicted to be more stable than the hepta- or octavalent species. Additionally, as opposed to Ge^{IV}, the divalent heterometals may not distort the symmetry of the structure. In Figure 3, the $ZnAl_{12}$ shows the smallest deviation from its mean M-O bond lengths, but is also situated quite far from the range of M-O bond lengths currently observed in the experimental clusters. In terms of the $FeAl_{12}$, the DFT calculations predict that all of the MAl_{12} clusters will have T_d symmetry with one exception, the high-spin Fe^{III} cluster which was converged with C_1 symmetry (See Tables S16 and S24 for Cartesian coordinates). Given the metastability in these clusters appears to arise partly due to strain at the tetrahedral core, introducing an open-shell transition metal will probably be difficult. To date there is one reported crystalline open-shell iron cluster adopting the Keggin structure - Bino et al., 2002, reported a fluorinated $FeFe_{12}$ cluster that adopts the ideal α-isomer of the Keggin structure with perfect T_d symmetry.

Adding a MAl_{12}^{6+} to the ε-Keggin structure library would be quite an accomplishment for this class of polyoxocations. Their lower total charge make them more stable relative to higher charged clusters according to the calculations, and this may just be enough to counteract any structural distortions that might occur from the larger heterometal placement in the restrictive aluminum cage. While we refrain from a lengthy discussion on possible competing species during the synthesis of these MAl_{12} clusters, this certainly is another consideration as to whether these theoretical species can be isolated. Many past attempts (Bino et al., 2002; Bradley et al., 1992; Kudynska et al., 1993; Lee et al., 2001; Nagy et al., 1995; Parker et al., 1997) aimed at

making new aluminum hydroxide clusters required successful crystallization to characterize the synthesis products. Recent advances in synthetic techniques and the ability to now characterize aqueous polynuclear species has led to a resurgence in this field. Methods in supramolecular chemistry that take advantage of the prevalence of hydrogen bonding present in the MAl_{12} clusters, have isolated new Keggin-type aluminum hydroxide clusters (Abeysinghe et al., 2012; Abeysinghe et al., 2013). Additionally, the γ-Al_{13} isomer of the Keggin structure was recently crystallized in a calcium-glycine system (Smart et al., 2013). Techniques such as electrospray-ionization mass spectroscopy can reveal successful synthesis prior to crystallization (Long et al., 2008; Son and Casey, 2013; Son et al., 2013) or when crystallization is unsuccessful.

Oxide dissolution and formation

This work shows that these structures are strained at their tetrahedral core compared to tetrahedral metal-oxo bonds in other structures and minerals. A finding that establishes these MAl_{12} clusters are not only metastable species with respect to other oxide and hydroxide minerals, but actually helps elucidate a key stabilizing structural characteristic in these polyoxocations. This finding is pertinent in terms of understanding how these particular structures interact with aqueous solutions, but also in the broader field of mineral oxide dissolution. Rate data collected on these substituted structures and other polyoxometalates has produced compelling evidence that surface ligand exchange, and subsequently oxide dissolution proceeds via metastable intermediates (Rustad and Casey, 2012; Rustad et al., 2004). As noted previously, the rates that these aluminum hydroxide clusters exchange bridging oxygens with a bulk solution is very sensitive to the nature of the heterometal. This sensitively is attributed to a mechanism that proceeds forming an intermediate by breaking overcoordinated oxygen bonds directly attached to the heterometal in the interior of the structure. The resulting loose dimer-like

structure allows addition of an isotopically normal oxygen to the newly undercoordinated metal via simple water exchanges in millisecond time scales. This oxygen scrambles as the intermediate collapses back into the stable molecular form. Our results in terms of the energetics of the structures follow the same pattern observed in their rates of exchange, supporting this mechanism for oxide dissolution.

Acknowledgements

The authors thank Dr. Jung-Ho Sung for his single-crystal structural refinements to confirm the $AlAl_{12}$ and $GaAl_{12}$ material identities. Support for the experimental thermochemical research was provided by the U.S. Department of Energy Office of Basic Energy Science via grant to AN DE-FG02-97ER14749. The DFT calculations were supported by a NSF CCI grant to WHC through the Center for Sustainable Materials Chemistry, grant CHE-11102637. Support for the synthesis and computation work was provided by the U.S. Department of Energy Office of Basic Energy Science via grant to WHC DE-FG02-05ER15693.

References

Abeysinghe, S., Unruh, D.K., and Forbes, T.Z. (2012) Crystallization of Keggin-Type Polyaluminum Species by Supramolecular Interactions with Disulfonate Anions. Crystal Growth & Design, 12(4), 2044-2051.

-. (2013) Surface Modification of Al30 Keggin-Type Polyaluminum Molecular Clusters. Inorganic Chemistry, 52(10), 5991-5999.

Allen, F. (2002) The Cambridge Structural Database: a quarter of a million crystal structures and rising. Acta Crystallographica Section B, 58(3 Part 1), 380-388.

Armstrong, C.R., Casey, W.H., and Navrotsky, A. (2011) Energetics of Al_{13} Keggin cluster compounds. Proc Natl Acad Sci, 108(36), 14775-15779.

Baker, L.C.W., and Figgis, J.S. (1970) New fundamental type of inorganic complex: hybrid between heteropoly and conventional coordination complexes. Possibilities for geometrical isomerisms in 11-, 12-, 17-, and 18-heteropoly derivatives. Journal of the American Chemical Society, 92(12), 3794-3797.

Becke, A.D. (1993) A new mixing of Hartree--Fock and local density-functional theories. The Journal of Chemical Physics, 98(2), 1372-1377.

Bino, A., Ardon, M., Lee, D., Spingler, B., and Lippard, S.J. (2002) Synthesis and Structure of [Fe13O4F24(OMe)12]5-: The First Open-Shell Keggin Ion. Journal of the American Chemical Society, 124(17), 4578-4579.

Bradley, S.M., Kydd, R.A., and Fyfe, C.A. (1992) Characterization of the galloaluminate GaO4Al12(OH)24(H2O)127+ polyoxocation by MAS NMR and infrared spectroscopies and powder x-ray diffraction. Inorganic Chemistry, 31(7), 1181-1185.

Casey, W.H., and Rustad, J.R. (2007) Reaction dynamics, molecular clusters and aqueous geochemistry. Annual Reviews of Earth Science, 35, 21-46.

Downs, R.T., and Palmer, D.C. (1994) The pressure behavior of alpha cristobalite. American Mineralogist, 79(1-2), 9-14.

Felsche, J. (1968) The alkali problem in the crystal structure of beta alumina. Zeitschrift für Kristallographie - Crystalline Materials, 127(1-4), 94-100.

Fleet, M. (1981) The structure of magnetite. Acta Crystallographica Section B, 37(4), 917-920.

Frisch, M.J., Trucks, G.W., Schlegel, H.B., Scuseria, G.E., Robb, M.A., Cheeseman, J.R., Scalmani, G., Barone, V., Mennucci, B., Petersson, G.A., Nakatsuji, H., Caricato, M., Li, X., Hratchian, H.P., Izmaylov, A.F., Bloino, J., Zheng, G., Sonnenberg, J.L., Hada, M., Ehara, M., Toyota, K., Fukuda, R., Hasegawa, J., Ishida, M., Nakajima, T., Honda, Y., Kitao, O., Nakai, H., Vreven, T., Montgomery, J.A., Peralta, J.E., Ogliaro, F., Bearpark, M., Heyd, J.J., Brothers, E., Kudin, K.N., Staroverov, V.N., Kobayashi, R., Normand, J., Raghavachari, K., Rendell, A., Burant, J.C., Iyengar, S.S., Tomasi, J., Cossi, M., Rega, N., Millam, J.M., Klene, M., Knox, J.E., Cross, J.B., Bakken, V., Adamo, C., Jaramillo, J., Gomperts, R., Stratmann, R.E., Yazyev, O., Austin, A.J., Cammi, R., Pomelli, C., Ochterski, J.W., Martin, R.L., Morokuma, K., Zakrzewski, V.G., Voth, G.A., Salvador, P., Dannenberg, J.J., Dapprich, S., Daniels, A.D., Farkas, Foresman, J.B., Ortiz, J.V., Cioslowski, J., and Fox, D.J. (2009) Gaussian 09, Revision B.01, Wallingford CT.

Furrer, G., Phillips, B.L., Ulrich, K.-U., Pöthig, R., and Casey, W.H. (2002) The origin of aluminum flocs in polluted streams. Science (New York, N.Y.), 297(5590), 2245-7.

Hazen, R.M., and Finger, L.W. (1986) High-pressure and high-temperature crystal chemistry of beryllium oxide. Journal of Applied Physics, 59(11), 3728-3733.

Johansson, G. (1960) On the Crystal Structures of Some Basic Aluminium Salts. Acta Chem. Scand., 14(3).

Keggin, J.F. (1933) Structure of the molecule of 12-phosphotungstic acid. Nature, 131(3321), 908-909.

Kudynska, J., Buckmaster, H.A., Kawano, K., Bradley, S.M., and Kydd, R.A. (1993) A 9 GHz cw-electron-paramagnetic resonance study of the sulphate salts of tridecameric [Mn[sub x]Al[sub 13 - x]O[sub 4](OH)[sub 24](H[sub 2]O)[sub 12]][sup (7 - x) +]. The Journal of Chemical Physics, 99(5), 3329-3334.

Lee, a.P., Phillips, B.L., Olmstead, M.M., and Casey, W.H. (2001) Synthesis and characterization of the GeO(4)Al(12)(OH)(24)(OH2)(12)(8+) polyoxocation. Inorganic Chemistry, 40(17), 4485-7.

Long, D.-L., Streb, C., Song, Y.-F., Mitchell, S., and Cronin, L. (2008) Unravelling the Complexities of Polyoxometalates in Solution Using Mass Spectrometry: Protonation versus Heteroatom Inclusion. Journal of the American Chemical Society, 130(6), 1830-1832.

Nagy, J.B., Bertrand, J.-C., Palinko, I., and Kiricsi, I. (1995) On the feasibility of iron or chromium substitution for aluminium in the Al13-Keggin ion. Journal of the Chemical Society, Chemical Communications, 0(22), 2269-2270.

Parker, W.O.N., Millini, R., and Kiricsi, I. (1997) Metal Substitution in Keggin-Type Tridecameric Aluminum−Oxo−Hydroxy Clusters. Inorganic Chemistry, 36(4), 571-575.

Popović, J., Tkalčec, E., Gržeta, B., Kurajica, S., and Rakvin, B. (2009) Inverse spinel structure of Co-doped gahnite. American Mineralogist, 94(5-6), 771-776.

Redfern, S.A.T., Harrison, R.J., O'Neill, H.S.C., and Wood, D.R.R. (1999) Thermodynamics and kinetics of cation ordering in MgAl 2 O 4 spinel up to 1600 degrees C from in situ neutron diffraction. American Mineralogist, 84(3), 299-310.

Rustad, J.R., and Casey, W.H. (2012) Metastable structures and isotope exchange reactions in polyoxometalate ions provide a molecular view of oxide dissolution. Nat Mater, 11, 223-226.

Rustad, J.R., Loring, J.S., and Casey, W.H. (2004) Oxygen-exchange pathways in aluminum polyoxocations. Geochimica et Cosmochimica Acta, 68(14), 3011-3017.

Smart, S.E., Vaughn, J., Pappas, I., and Pan, L. (2013) Controlled step-wise isomerization of the Keggin-type Al13 and determination of the [gamma]-Al13 structure. Chemical Communications, 49(97), 11352-11354.

Smith, G.S., and Isaacs, P.B. (1964) The crystal structure of quartz-like GeO2. Acta Crystallographica, 17(7), 842-846.

Son, J.-H., and Casey, W.H. (2013) A decatungstate-type polyoxoniobate with centered manganese: [H2MnIVNb10O32]8- as a soluble tetramethylammonium salt. Dalton Transactions, 42(37), 13339-13342.

Son, J.-H., Ohlin, C.A., Johnson, R.L., Yu, P., and Casey, W.H. (2013) A Soluble Phosphorus-Centered Keggin Polyoxoniobate with Bicapping Vanadyl Groups. Chemistry – A European Journal, 19(16), 5191-5197.

Sousa, S.F., Fernandes, P.A., and Ramos, M.J. (2007) General Performance of Density Functionals. The Journal of Physical Chemistry A, 111(42), 10439-10452.

Stephens, P.J., Devlin, F.J., Chabalowski, C.F., and Frisch, M.J. (1994) Ab Initio Calculation of Vibrational Absorption and Circular Dichroism Spectra Using Density Functional Force Fields. The Journal of Physical Chemistry, 98(45), 11623-11627.

Stewart, T., A., Trudell, D., E., Alam, T., M., Ohlin, C.A., Lawler, C., Casey, W., H., Jett, S., and Nyman, M. (2009) Enhanced water purification: a single atom makes a difference. Environ Sci Technol, 43(14), 5416-22.

Vosko, S.H., Wilk, L., and Nusair, M. (1980) Accurate spin-dependent electron liquid correlation energies for local spin density calculations: a critical analysis. Canadian Journal of Physics, 58(8), 1200-1211.

Wong, M.W. (1996) Vibrational frequency prediction using density functional theory. Chemical Physics Letters, 256(4–5), 391-399.

Zhao, Y., and Truhlar, D.G. (2008) Density Functionals with Broad Applicability in Chemistry. Accounts of Chemical Research, 41(2), 157-167.

Zinkevich, M., Morales, F.M., Nitsche, H., Ahrens, M., Rühle, M., and Aldinger, F. (2004) Microstructural and thermodynamic study of γ-Ga₂O₃. Zeitschrift für Metallkunde, 95, 756 - 762.

Figure Captions

Figure 1. Polyhedral representation of the tridecameric cluster having the structure of the ε-isomer of the Baker-Figgis-Keggin series and the stoichiometry: $[MO_4Al_{12}(OH)_{24}(OH_2)_{12}]^{6/7/8+}$. The tetrahedral core, M^{x+} is orange and the octahedrally coordinated aluminum cations are blue.

Figure 2. (a.) The clipped representation of MAl_{12} cluster to display local bonding environment. One full aluminum trimeric group with pink atoms is shown bonded to the tetrahedral metal center, orange. We show the geometric consideration used in Figure 2b, represented as the distance, *d*, between the heterometal to the trimeric group plane. (b.) ΔH_{ex}, with the $GeAl_{12}$ cluster is plotted as a function of *d* in Figure 2a. Results are shown for both experimental MAl_{12} solid clusters and the b3lyp/6-31g*/PCM calculated aqueous clusters.

Figure 3. Distribution of average M-O bond lengths in dozens to hundreds of tetrahedrally coordinated structures (109.47 ± 3°) observed in the Cambridge Crystal Structure Database (CCSD)(Allen, 2002). All M-O bond lengths from the mineral structures in Table 3 lie within these distributions. The MAl_{12} M-O bond lengths calculated using the LDA method (Table 2) are overlaid for comparison. The LDA method results compare well with the experimental results obtained from the $GaAl_{12}$, $AlAl_{12}$, and $GeAl_{12}$ clusters, with a mean absolute error (MAE) of 0.01 Å. The differences are well beyond the calculation inaccuracy.

Tables

Table 1. Summary of calorimetric data for MAl_{12} selenates and the tetrahedral bond lengths, <M-O>, for the substituted heterometal.

MAl_{12}	<M-O> (Å)	ΔH_{soln} in 5 N HCl (kJ·mol^{-1})	$\Delta H^{\circ}_{f,el}$ (kJ·mol^{-1})[c]

$GaAl_{12}$	1.88[a] (1.879[b])	-869.71 ± 5.18 (9)	-23,075.02 ± 61.68
$AlAl_{12}$	1.83[a] (1.831[b])	-958.04 ± 2.79 (8)	-23,334.18 ± 60.38
$GeAl_{12}$	1.81[c]	-975.19 ± 11.52[d](8)	-

Notes: [a]this work SXRD refinements; [b](Parker et al., 1997); [c](Lee et al., 2001); [d]$\Delta H_{soln}(GeAl_{12})$ was calculated using the thermodynamic cycle in Table S3 with two decimal places kept to minimize roundoff error. The number of experiments are in parentheses.; [c]$\Delta H^{\circ}_{f,el}$ ($Na[(MO_4)Al_{12}(OH)_{24}(H_2O)_{12}](SeO_4)_4 \cdot 12H_2O_{(cr)}$) was calculated using the thermodynamic cycle in Table S1.

Table 2. Summary of DFT structural data and energies. Experimental bond lengths from Table 1 are shown in parenthesis for comparison.

MAl_{12}	**PCM b3lyp <M-O> (Å)**	**PCM SVWN5 <M-O> (Å)**	**PCM b3lyp ΔH_{ex} with $GeAl_{12}^{8+}$ ($kJ \cdot mol^{-1}$)**	**Gas b3lyp ΔH_{ex} with $GeAl_{12}^{8+}$ ($kJ \cdot mol^{-1}$)**
$ZnAl_{12}$	2.05	1.96	-432.21	-4263.27
$MgAl_{12}$	2.03	1.99	-403.53	-4233.58
$BeAl_{12}$	1.83	1.79	-283.10	-4125.29
$GaAl_{12}$	1.92	1.89 (1.88)	-151.80	-1989.79
$FeAl_{12}$	1.94[a]	1.89[a]	-76.85	-1934.32
$AlAl_{12}$	1.86	1.84 (1.83)	-37.23	-1868.19
$GeAl_{12}$	1.82	1.81 (1.82)[c]	Defined, 0	Defined, 0
$SiAl_{12}$	1.73	1.71	264.05	208.76

[b]MAE	0.03	0.01	-33.20	-

458 Notes: [a]$FeAl_{12}$ bond lengths are the average <M-O> bond lengths. [b]MAE, is calculated for the
459 three experimental clusters for bond lengths and the two experimental clusters, $GaAl_{12,}$ and
460 $AlAl_{12}$, for ΔH_{ex} with $GeAl_{12}^{8+}$; [c](Lee et al., 2001).

461

462 **Table 3.** Selected tetrahedral M-O bond lengths and O-M-O angles in minerals compared to the
463 corresponding calculated MAl_{12} using the SVWN5/6-31g*/PCM method. Values in parenthesis
464 are experimental.

Mineral	O-T-O angle (degrees)	<M-O> (Å)	MAl_{12} <M-O> (Å)
Zn: Gahnite ($ZnAl_2O_4$)[a]	109.47	1.95	1.96
Mg: Spinel ($MgAl_2O_4$)[b]	109.47	1.91	1.99
Be: Bromellite (BeO)[c]	108.93-110.03	1.65-1.66	1.79
Ga: Gallium Oxide (γ-Ga_2O_3)[d]	109.47	1.78	1.89 (1.88)
Fe: Magnetite (Fe_3O_4)[e]	109.47	1.89	1.89[i]
Al: Na-β-alumina ($NaAl_2O_3$)[f]	107.09-111.76	1.75	1.84 (1.83)
Ge: β-Quartz-Type (GeO_2)[g]	106.30-113.10	1.74	1.81 (1.81)
Si: Crystobalite (SiO_2)[h]	109.02-111.42	1.60	1.71

Notes: [a](Popović et al., 2009); [b](Redfern et al., 1999); [c](Hazen and Finger, 1986);[d](Zinkevich et al., 2004);[e](Fleet, 1981);[f](Felsche, 1968); [g](Smith and Isaacs, 1964); [h](Downs and Palmer, 1994); [i]$FeAl_{12}$ bond lengths are given as an average of the four M-O bond lengths.

Figures

Figure 1

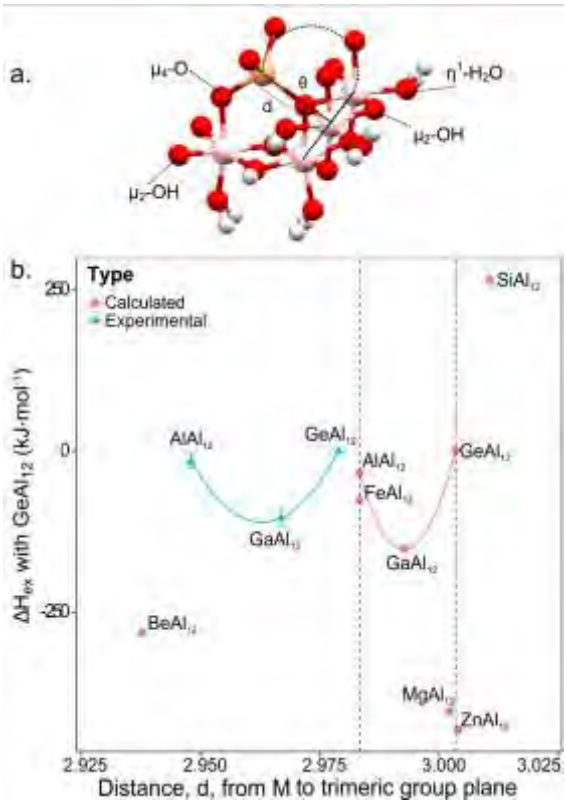

473

474 **Figure 2**

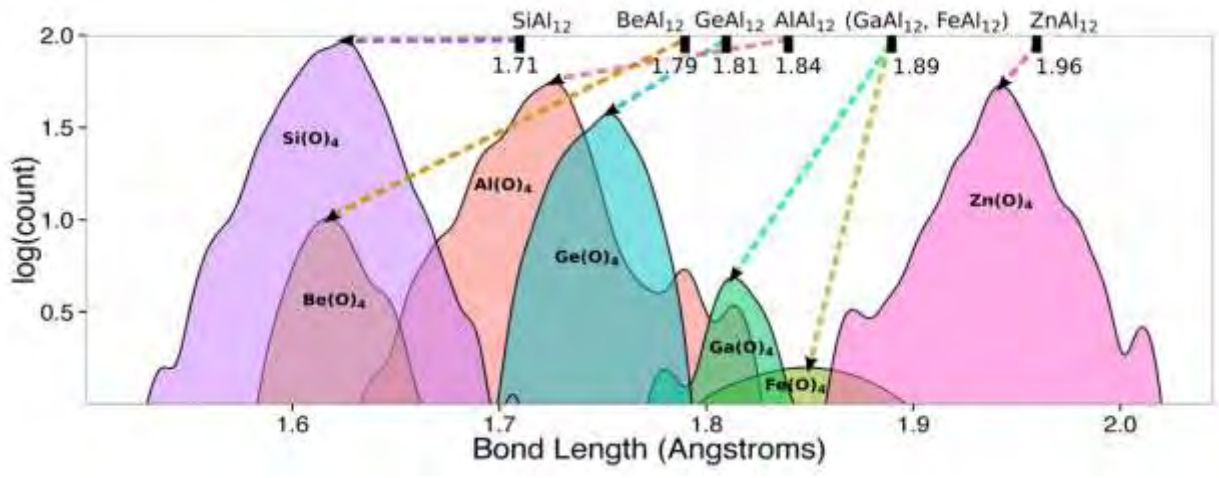

475

476 **Figure 3**